Journal of Alloys and Compounds 509 (2011) 7381–7388

Contents lists available at ScienceDirect

Journal of Alloys and Compounds

journal homepage: www.elsevier.com/locate/jallcom

EPR studies of (Bi, Pb)-2223 phase substituted by Ruthenium ions

A.I. Abou-Aly, R. Awad*, S.A. Mahmoud, M.ME. Barakat

Physics Department, Faculty of Science, Alexandria University, Alexandria, Egypt

ARTICLE INFO

Article history:
Received 20 December 2010
Received in revised form 28 March 2011
Accepted 29 March 2011
Available online 5 April 2011

Keywords:
(Bi, Pb)-2223 phase
Ru-content
EPR
Curie temperature

ABSTRACT

This work studied X-ray powder diffraction (XRD), electrical resistivity and electron paramagnetic resonance (EPR) measurements for $Bi_{1.8}Pb_{0.4}Sr_2Ca_{2.1}Cu_{3-x}Ru_xO_{10+\delta}$ ($0.0 \le x \le 0.4$) superconducting samples. XRD analysis and electrical resistivity data showed that the low-content of Ru, $x \le 0.05$, enhanced both the phase formation and the superconducting transition temperature of (Bi, Pb)-2223 phase. A phase change from (Bi, Pb)-2223 phase to (Bi, Pb)-2212 phase was reported for $x \ge 0.15$. Two EPR lines were observed for $0.0 \le x \le 0.075$, indicating the presence of both (Bi, Pb)-2223 and (Bi, Pb)-2212 phases. While, one EPR line was observed for $x \ge 0.15$, corresponding to the (Bi, Pb)-2212 phase formation. The number of spins (N) participating in the resonance and its spin paramagnetic susceptibility (χ), for the two phases, were calculated as a function of both Ru-content and temperature. In addition, we reported the variation of activation energy (E_a), Curie constant (C), Curie temperature (θ) and effective magnetic moment (μ) with Ru-content.

1. Introduction

Among the high-temperature superconducting materials (HTSCs), the Bi-2223 phase is considered as the most promising one to synthesis tapes and wires for large-scale and high-current applications [1]. It is characterized by high superconducting transition temperature T_c, critical current density J_c and upper critical magnetic B_{c2} of order 110 K, 8000 A/cm^2 and 150 T, respectively [2]. Tremendous works [3–5] were directed towards the preparation of Bi-2223 phase as a single phase in order to optimize its T_c. The formation of Bi-2223 phase strongly depends on the preparation conditions such as sintering temperature, thermal processing time, synthesis atmosphere, precursor compositions and substitution with various cations and anions. The best results revealed that the formation of Bi-2223 phase was significantly enhanced through the partial substitution of Bi by Pb [6]. Many methods were carried out to prepare (Bi, Pb)-2223 superconducting phase including conventional solid-state reaction [7], co-precipitation [8], sol–gel [9,10] and micro-emulsion-based techniques [11]. The simplest one is the conventional solid-state reaction technique which gives good results after optimizing its preparation conditions. The (Bi, Pb)-2223 phase is also extremely difficult to prepare as a single phase as it usually intergrowths with the (Bi, Pb)-2212 phase. However, this is due to the high complexity of the reaction and the small difference in their thermodynamic stabilities [12].It is well known that the chemical substitutions or additions play an important role for knowing the origin and the structure of HTSCs. The substitution of Mg in Ca-site showed reduction in both the intergranular coupling and critical current density for (Bi, Pb)-2223 phase by increasing Mg-content [13]. Terzioglu et al. [14] studied the effect of Sm substitution in $Bi_{1.6}Pb_{0.4}Sr_2Ca_{2-x}Sm_xCu_3O_{10+\delta}$ phase. The decrease in the hole carriers concentration resulted in the suppression of T_c and J_c. A phase change from (Bi, Pb)-2223 phase to (Bi, Pb)-2212 phase was also observed for $x \ge 0.1$. Increasing of Cd-content up to 0.04 in $Bi_{1.64}Pb_{0.36}Sr_2Ca_{2-x}Cd_xCu_3O_{10+\delta}$ phase, with annealing time of 270 h, increased the phase volume fraction, T_c, J_c and flux pinning energy [15]. A phase change from (Bi, Pb)-2223 phase to (Bi, Pb)-2212 phase was observed at $x \ge 0.1$ due to the formation of weak links. Abou-Aly et al. [16] reported the enhancement of the phase volume fraction, T_c, flux pinning energy, J_c and B_{c2} in $Bi_{1.8}Pb_{0.4}Sr_2Ca_{2.1}Cu_{3-x}Ru_xO_{10+\delta}$ phase up to $x = 0.05$. Beyond which they decreased with further increase in Ru-content and a phase change from (Bi, Pb)-2223 phase to (Bi, Pb)-2212 phase was occurred for $x \ge 0.15$. On the other hand, the addition of Gd in $Bi_{1.8}Pb_{0.35}Sr_{1.9}Ca_{2.1}Cu_3Gd_xO_{10+\delta}$ phase decreased both T_c and J_c [17]. The surface morphology and grain connectivity were degraded, meanwhile (Bi, Pb)-2223 phase disappeared and only (Bi, Pb)-2212 phase was observed at $x \ge 0.3$. While, the maximum phase volume fraction, T_c and J_c were reported as a result of 0.5 wt.% Cr_2O_3 addition in (Bi, Pb)-2223 phase [18], but the excessive addition of Cr_2O_3 degraded the superconductivity of this phase.

One of the rare techniques used to investigate the properties of high-temperature superconductors is the electron paramagnetic resonance (EPR). This is due to the presence of difficulties through the measurement and the interpretation of the results. These diffi-

* Corresponding author. Tel.: +203 5759086.
E-mail address: rawad64@yahoo.com (R. Awad).

0925-8388/$ – see front matter © 2011 Elsevier B.V. All rights reserved.
doi:10.1016/j.jallcom.2011.03.160

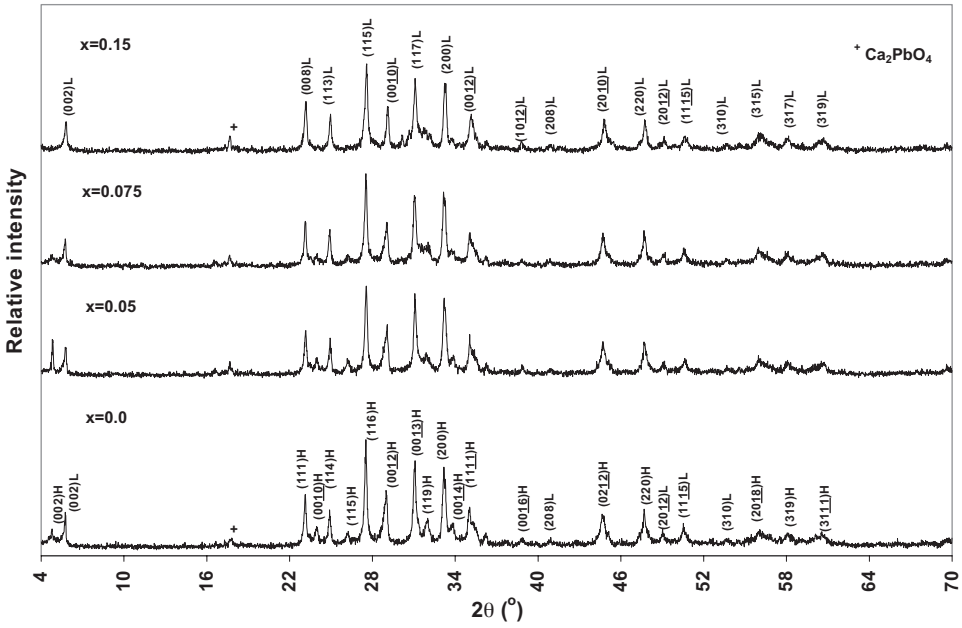

Fig. 1. XRD patterns for $Bi_{1.8}Pb_{0.4}Sr_2Ca_{2.1}Cu_{3-x}Ru_xO_{10+\delta}$, with $x = 0.0$, 0.05, 0.075 and 0.15.

culties arise from temperature adjustment, a fixed phase of lock-in detector spectrometer with respect to the ac phase and probe the microwave dissipation as a function of the sweeping magnetic field [19]. However, EPR is potentially a powerful tool in HTSCs for examining the magnetic origin, and giving the information about the structure, the *g*-value of spin from the resonance field, the line width and its intensity, the number of spins participating in the resonance and the paramagnetic susceptibility via the first derivative EPR absorption spectra. The EPR signal of HTSCs arises from the bulk Cu^{2+} ions with spin $S = 1/2$ and depends on the preparation conditions, doping level and samples homogeneity [20]. Therefore, EPR technique is treated as an indication of the degree of purity. The anisotropic *g*-factors, g_x, g_y and g_z, for the orthorhombic Co^{2+} center on the Cu(1) site in $YBa_2Cu_{2.7}Co_{0.3}O_{7-\delta}$ at room temperature were investigated theoretically by Wu et al. [21]. The pronounced decrease in the intensity and the remarkable nonlinear increase in the g_y of Co^{2+} EPR spectra were observed by decreasing the temperature from room temperature to 150 K. Bejjit et al. [22] reported the EPR spectra at different temperatures (4–300 K) for $GdBa_2Cu_3O_7$ single crystal, before and after grinding. The EPR line for single crystal, in the normal state, was isotropic and asymmetrical due to the skin effect. On the contrary, it was characterized by a non-resonant spectra and the noise in the spectrum in the superconducting state. After grinding of the single crystal, the skin effect was eliminated and the EPR line became symmetrical. The effect of oxygen-content in the localized spin moment of Cu^{2+} ions, from electron spin resonance ESR, in $Bi_2Sr_2CaCu_2O_{8+\delta}$ single crystal was studied by Li et al. [23]. ESR signals decreased with increasing oxygen-content from under-doped to over-doped region.

In this work, the EPR results of $Bi_{1.8}Pb_{0.4}Sr_2Ca_{2.1}Cu_{3-x}Ru_xO_{10+\delta}$ superconducting phase ($0.0 \le x \le 0.4$) were measured in the normal-state. The results of EPR were discussed with respect to the composition as well as the temperature and correlated with those obtained from XRD and electrical resistivity [16].

2. Experimental details

Conventional solid-state reaction technique was used to prepare superconducting samples of the nominal composition $Bi_{1.8}Pb_{0.4}Sr_2Ca_{2.1}Cu_{3-x}Ru_xO_{10+\delta}$, with $x = 0.0$, 0.025, 0.05, 0.075, 0.15, 0.3 and 0.4. The starting materials were Bi_2O_3, PbO, $SrCO_3$, CaO, CuO and RuO_2 (purity ≥ 99.9). The starting powder was crushed manually in an agate mortar, sifted using a 125 μm sieve and subjected to calcinations process in air at 820 °C for 24 h to remove any remaining volatile materials. After cooling, the resulting powder was ground, sifted using the same sieve and then pressed in the form of disc (1.5 cm in diameter and 0.3 cm in thickness). Discs were sintered in air at 845 °C with a heating rate 4 °C/min, and held at this temperature for 96 h. Finally the samples were cooled with a rate of 2 °C/min to room temperature.

The prepared samples were characterized by XRD using Shimadzu-7000 powder diffractometer with Cu-K_α radiation ($\lambda = 1.54056$ Å) in the range $4° \le 2\theta \le 70°$. The electrical resistivity of the prepared samples was measured by a conventional four-probe technique from room temperature down to zero resistivity temperature (T_o) with a closed cryogenic refrigeration system. The samples used for resistivity measurements had dimensions of about 1.5 cm × 0.2 cm × 0.3 cm, and the copper leads to the samples were made using a conductive silver paint. The temperature of the samples was monitored by a Chromel versus Fe–Au thermocouple and stabilized with the aid of a temperature controller to within ±0.1 K.

The EPR spectra were performed using a Bruker Elexsys 500 EPR spectrometer operating at the X-band frequency (≈9.491 GHz) with a field modulation frequency of 100 kHz. The magnetic field was scanned in the range 500–6500 G and the used microwave power was 0.64 mW. A powder sample of 100 mg was taken in a quartz tube for EPR measurements. The EPR spectra of the prepared samples were recorded at different temperatures (120–290 K). A temperature stability of ±1 K was obtained using temperature controller (Bruker ER-4131).

3. Results and discussion

Fig. 1 shows the XRD patterns for $Bi_{1.8}Pb_{0.4}Sr_2Ca_{2.1}Cu_{3-x}Ru_xO_{10+\delta}$, with $x = 0.0$, 0.025, 0.075 and 0.15. It is observed for $x = 0.0$ that the most high-intensities peaks belong to a nearly single tetragonal phase of (Bi, Pb)-2223 with few low-intensities peaks which belong to (Bi, Pb)-2212 and Ca_2PbO_4 phases. The (Bi, Pb)-2223 peaks are indicated by H (*h k l*), those of (Bi, Pb)-2212 phase are indicated by *L* (*h k l*) and of Ca_2PbO_4 phase is indicated by (+). It is found that the intensities of peaks, which correspond to (Bi, Pb)-2223 phase, are enhanced for low Ru-content, $0.0 < x \le 0.05$, as observed in the typical peak of (Bi, Pb)-2223 phase at $2\theta = 4.77°$. This indicates that the low Ru-content enhances the formation of (Bi, Pb)-2223 phase, meaning that Ru is considered as one of the elements which stabilizes (Bi, Pb)-2223 phase. This peak decreases at $x = 0.075$ and the intensities of peaks which belong to (Bi, Pb)-2212 phase increase. For $x \ge 0.15$, (Bi, Pb)-2223 phase patterns completely disappeared and only those belonging to (Bi, Pb)-2212 and Ca_2PbO_4 phases predominated. These results show that the high Ru-content degrades the formation of (Bi, Pb)-2223 phase and favors the formation of (Bi, Pb)-2212 phase. The volume fraction

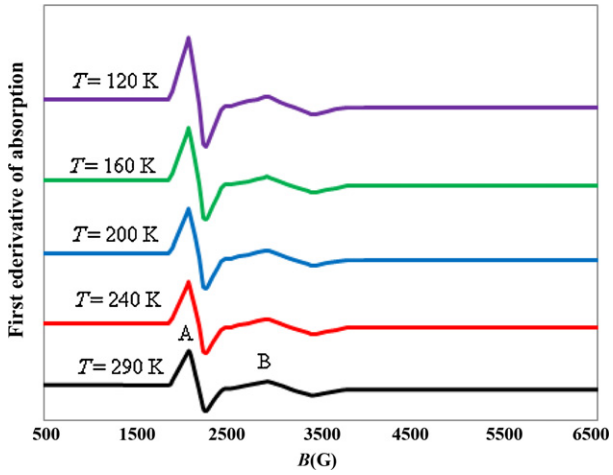

Fig. 2. The first derivative EPR absorption spectra of $Bi_{1.8}Pb_{0.4}Sr_2Ca_{2.1}Cu_{3-x}Ru_xO_{10+\delta}$ versus the magnetic field at different temperatures.

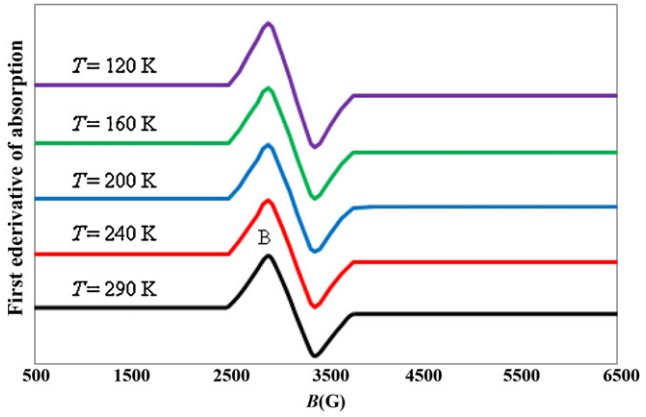

Fig. 3. The first derivative EPR absorption spectra of $Bi_{1.8}Pb_{0.4}Sr_2Ca_{2.1}Cu_{3-x}Ru_xO_{10+\delta}$ versus the magnetic field at different temperatures.

of (Bi, Pb)-2223, (Bi, Pb)-2212 and Ca_2PbO_4 phases were calculated through Eqs. (1)–(3), respectively.

$$\text{(Bi, Pb)-2223(\%)} = \frac{\sum I_{2223}}{\sum I_{2223} + \sum I_{2212} + \sum I_{Ca_2PbO_4}} \times 100\% \quad (1)$$

$$\text{(Bi, Pb)-2212(\%)} = \frac{\sum I_{2212}}{\sum I_{2223} + \sum I_{2212} + \sum I_{Ca_2PbO_4}} \times 100\% \quad (2)$$

and

$$Ca_2PbO_4(\%) = \frac{\sum I_{Ca_2PbO_4}}{\sum I_{2223} + \sum I_{2212} + \sum I_{Ca_2PbO_4}} \times 100\% \quad (3)$$

where I is the peak intensity of the present phases. The volume fraction of (Bi, Pb)-2223, (Bi, Pb)-2212 and Ca_2PbO_4 phases, as well as the superconducting transition temperature which was determined from electrical resistivity measurement [16], for $Bi_{1.8}Pb_{0.4}Sr_2Ca_{2.1}Cu_{3-x}Ru_xO_{10+\delta}$ are listed in Table 1. The volume fraction of (Bi, Pb)-2223 phase and the superconducting transition temperature increase as x increases from 0.0 to 0.05, whereas they have a reverse trend with further increase in x. The volume fraction of (Bi, Pb)-2212 and Ca_2PbO_4 phases decrease as x increases from 0.0 to 0.05 and then they increase with further increase in x. A phase change from (Bi, Pb)-2223 phase to (Bi, Pb)-2212 phase was observed at $x \geq 0.15$ [16]. This phase change might be due to the distortion between (Bi, Pb)-2223 slabs and the formation of weak links at grain boundaries, leading to a gradual decrease in the T_c through the high partial substitution of Cu^{2+} ions by Ru^{4+} ions.

Fig. 2 shows the first derivative EPR absorption spectra for $Bi_{1.8}Pb_{0.4}Sr_2Ca_{2.1}Cu_{3-x}Ru_xO_{10+\delta}$ at different temperatures T = 290, 240, 200, 160 and 120 K. It is clear that the EPR spectra contain two isotropic lines, indicating the formation of both (Bi, Pb)-2223 and (Bi, Pb)-2212 phases. These lines are labeled by A and B for (Bi, Pb)-2223 and (Bi, Pb)-2212 phases, respectively. Similar results were observed by Owens et al. [24] in $Bi_{1.5}Pb_{0.5}Sr_2Ca_{n-1}Cu_nO_{2n+4+\delta}$ superconductors. This behavior is attributed to point defects which are localized on copper–oxygen complexes at dislocations in the boundary region between the intergrowth of both (Bi, Pb)-2223 and (Bi, Pb)-2212 phases. Also, the two isotropic EPR lines A and B are attributed to the outer pyramidal CuO_2-planes in the boundary region, which are responsible for the electrical conduction in both normal and superconducting states. The linkage between the Cu^{2+} ions allows for the magnetic exchange interaction between them in the CuO_2-planes. Each isotropic EPR line is symmetric about its central position. This symmetric shape indicates the absence of skin effect, meaning that the powder grain-size is smaller than skin-depth [22]. It should be noted that the broadening of line B is greater than that of line A. This broadening may be attributed to the magnetic dipolar interactions between Cu^{2+} ions in CuO_2-planes which are higher in (Bi, Pb)-2212 phase than those in (Bi, Pb)-2223 phase. Similar EPR spectra, at different temperatures, were detected for $Bi_{1.8}Pb_{0.4}Sr_2Ca_{2.1}Cu_{3-x}Ru_xO_{10+\delta}$, ($x$ = 0.025, 0.05 and 0.075) with different intensities and line widths. By increasing Ru-content, $x \geq 0.15$, the EPR line A disappears and only EPR line B is observed, as shown in Fig. 3 for x = 0.15 at different temperatures (290–120 K). The disappearance of the EPR line A indicates the complete conversion of (Bi, Pb)-2223 phase to (Bi, Pb)-2212 phase.

In order to confirm this phase change, the variation of the first derivative EPR absorption spectra versus the magnetic field for $Bi_{1.8}Pb_{0.4}Sr_2Ca_{2.1}Cu_{3-x}Ru_xO_{10+\delta}$, $0.0 \leq x \leq 0.4$ is plotted in Fig. 4(a) and (b) at T = 290 and 120 K, respectively. It is clear that as x increases from 0.0 to 0.075 the two lines A and B appear, indicating the presence of both (Bi, Pb)-2223 and (Bi, Pb)-2212 phases. For $x \geq 0.15$ only the line B appears whereas the line A disappears. This indicates that higher Ru-content could produce a phase change from (Bi, Pb)-2223 phase to (Bi, Pb)-2212 phase. These results are consistent with the previous data obtained from XRD and electrical resistivity measurements [16]. It is important to mention that the ferromagnetic resonance line FMR corresponding to Ru^{4+} ions below T_N = 133 K, originated from the Ru moments in RuO_2 layers [25], does not appear until x = 0.4. The ferromagnetic order is caused by an antisymmetric exchange coupling between neighboring Ru moments. This is induced by a local distortion that breaks the tetragonal symmetry of RuO_6 octahedral. The disappearance of FMR line confirms the electrical resistivity data [16] which did not show an upturn in the resistivity data at T_N = 133 K. The lines of EPR spectra show a slight shift as the temperature decreases from room temperature to 120 K, leading to a slight change in the g-values. The relative measurements of g-values, for each phase at different temperatures, can be calculated against the standard ($CuSO_4 \cdot 5H_2O$ in this study) of known g-values using Eq. (4) [26]. This equation is considered as a useful tool in the case of spin concentration measurements and it includes the experimental parameters of the used sample, subscript y, and standard, subscript $std.$:

$$g_y - g_{std} = -\frac{B_y - B_{std}}{B_{std}} g_{std} \quad (4)$$

where B is the center-field position of the EPR spectrum. The variation of g-values for (Bi, Pb)-2223 and (Bi, Pb)-2212 phases with temperature is shown in Fig. 5(a) and (b), respectively. They have a slight temperature dependence, which may be related to the dynamic Jahn–Teller (JT) effect in these compounds [27,28]. The

Table 1
The variation of volume fraction of (Bi, Pb)-2223, (Bi, Pb)-2212 and Ca_2PbO_4 phases, T_c and the ratio of both volume fraction and area for (Bi, Pb)-2223 phase to those for (Bi, Pb)-2212 phase with Ru-content.

x	Volume fraction			T_c (K)	The ratio of (Bi, Pb)-2223 phase to (Bi, Pb)-2212 phase	
	(Bi, Pb)-2223 phase	(Bi, Pb)-2212 phase	Ca_2PbO_4 phase		Volume fraction	Area
0.0	86.37	12.59	1.04	103.50	6.86	6.75
0.025	87.95	10.64	1.41	104.75	8.27	8.14
0.05	88.84	10.22	0.94	106.00	8.69	9.17
0.075	73.17	25.57	1.26	99.75	2.86	2.81
0.15	–	96.92	3.08	66.63	–	–
0.3	–	95.61	4.39	50.50	–	–
0.4	–	95.66	4.34	–	–	–

calculated g-values for both (Bi, Pb)-2223 and (Bi, Pb)-2212 phases are greater than those that were determined by Owens et al. [24]. This is probably due to the different environmental conditions of Cu^{2+} ions. Also, the difference in g-values of Cu^{2+} ions in (Bi, Pb)-2223 and (Bi, Pb)-2212 phases is attributed to the difference in the electronic structure of CuO_2-planes, resulting from the difference in the number of isolating planes between CuO_2-planes.

The relative intensity as a function of temperature for (Bi, Pb)-2223 and (Bi, Pb)-2212 phases is shown in Fig. 6(a) and (b), respectively. The EPR line intensity increases as the temperature decreases from room temperature to 120 K. This obeys the Curie–Weiss law for simple paramagnetic centers, indicating the isolated nature of the corresponding Cu^{2+} ions centers which does seem to interact significantly with its environment. As Ru-content increases from 0.0 to 0.05, the EPR relative intensity for (Bi, Pb)-2223 phase increases and then it decreases at $x = 0.075$. On contrary, the EPR relative intensity for (Bi, Pb)-2212 phase decreases until $x = 0.05$ and it increases with further increase in x. This means that lower content of Ru enhances the unpaired electrons in the CuO_2-planes in (Bi, Pb)-2223 phase and reduces them in (Bi, Pb)-2212 phase. These results are well correlated with the volume fraction of each phase, indicating a phase change from (Bi, Pb)-2223 phase to (Bi, Pb)-2212 phase for $x \geq 0.15$.

The temperature dependence of the peak-to-peak line width (Δx_{pp}) is shown in Fig. 7(a) and (b) for (Bi, Pb)-2223 and (Bi, Pb)-2212 phases, respectively. We observe a linear decrease when the temperature decreases from room temperature to 120 K. This behavior is quite similar to that observed for the high-temperature superconductors above the superconducting transition temperature [22]. The temperature dependence of the peak-to-peak line width can be fitted by:

$$\Delta x_{pp} = A_{pp} + B_{pp}T \quad (5)$$

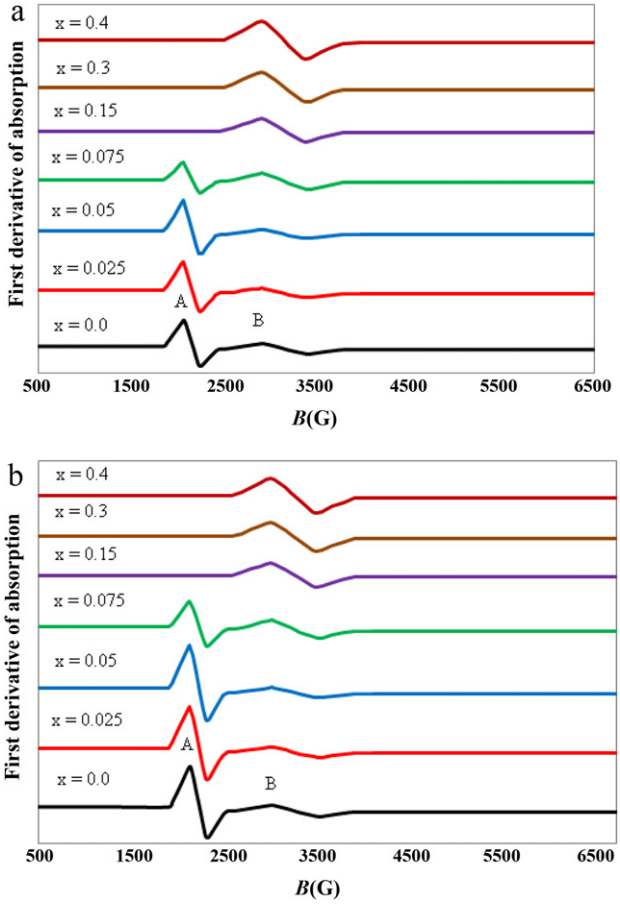

Fig. 4. The first derivative EPR absorption spectra versus the magnetic field for $Bi_{1.8}Pb_{0.4}Sr_2Ca_{2.1}Cu_{3-x}Ru_xO_{10+\delta}$ ($0.0 \leq x \leq 0.4$), at $T = 290$ K (a) and $T = 120$ K (b).

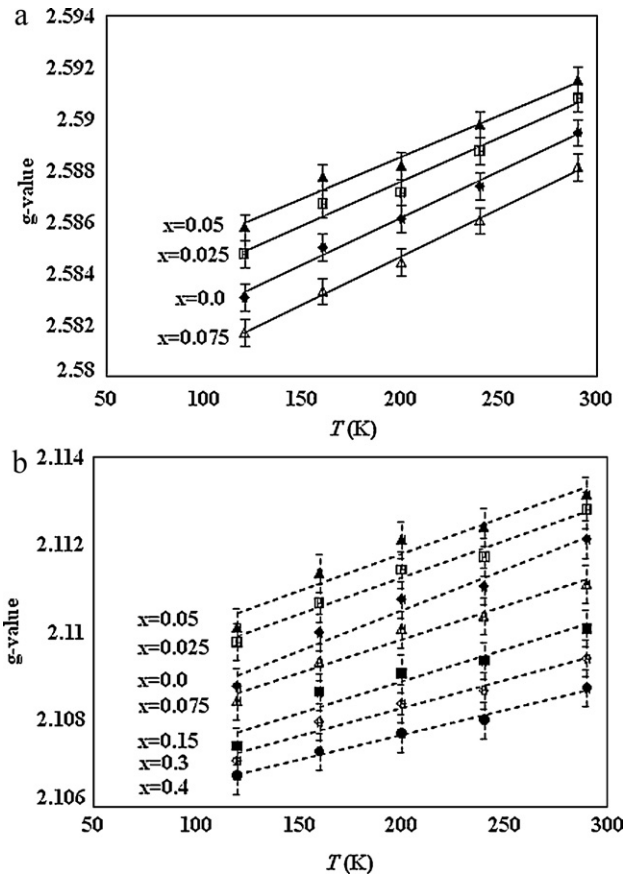

Fig. 5. The variation of g-values with temperature for different Ru-content for (Bi, Pb)-2223 phase (a), and (Bi, Pb)-2212 phase (b).

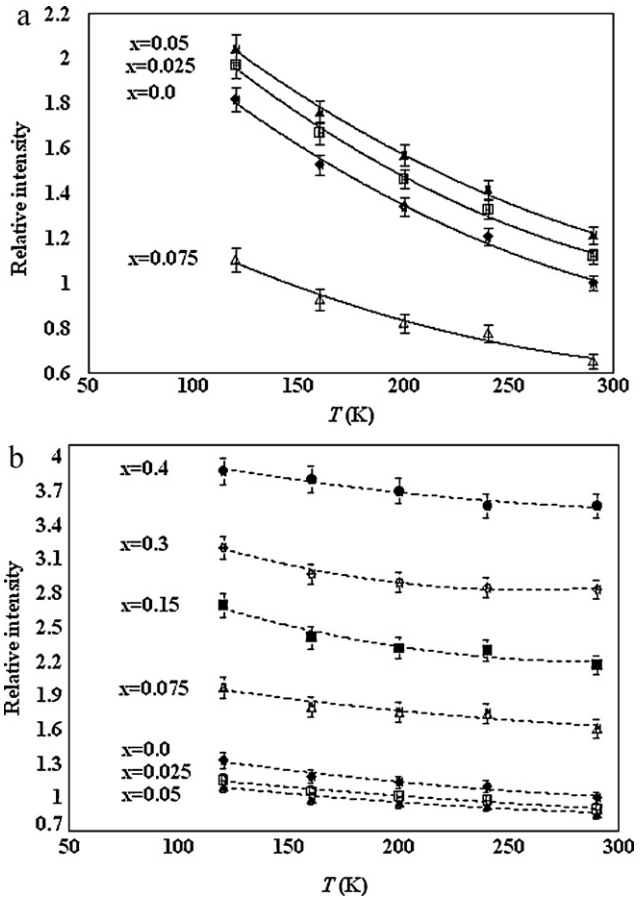

Fig. 6. The relative intensity variation with temperature for different Ru-content for (Bi, Pb)-2223 phase (a), and (Bi, Pb)-2212 phase (b).

where A_{pp} is the residual line width which is closely connected with the molecular field at the Cu-site and B_{pp} is the thermal broadening, corresponding to the Korringa-type interaction between either Cu^{2+} ions or Ru^{4+} ions with the host conduction carriers through the exchange interactions J_s [29]. The fitting parameters A_{pp} and B_{pp} are listed in Table 2 with Ru-content for both (Bi, Pb)-2223 and (Bi, Pb)-2212 phases. It is noticed that the value of A_{pp} decreases as x increases from 0.0 to 0.05 and then it increases when $x = 0.075$ for (Bi, Pb)-2223 phase. For (Bi, Pb)-2212 phase, A_{pp} increases until $x = 0.05$ and then it decreases with further increase in x. This means that the residual line width could depend on the volume fraction for both (Bi, Pb)-2223 and (Bi, Pb)-2212 phases. This behavior may be also responsible for the relative intensity behavior for each phase with increasing Ru-content. The data in Table 2 indicates that the value of B_{pp} increases, for (Bi, Pb)-2223 phase, until $x = 0.05$ and then decreases for $x = 0.075$. This behavior is quite similar to that of the variation of hole density with Ru-content [16]. On the other hand for (Bi, Pb)-2212 phase, the fitting parameter B_{pp} shows a decrement in its value as Ru-content increases. The fitting parameter B_{pp} is expressed by [30]:

$$B_{pp} = \left(\frac{8\pi^2 k_B}{\gamma h}\right) [J_s N(E_F)]^2 \quad (6)$$

where $N(E_F)$ is the density of state at the Fermi level, k_B is Boltzmann's constant, h is Planck constant and γ is the gyromagnetic ratio. Since the density of state is directly proportional to the number of carriers, so the value of $B_{pp}^{1/2}$ is proportional to the number of carriers in the CuO_2-planes. Increasing the B_{pp} value with increasing Ru-content from 0.0 to 0.05, for (Bi, Pb)-2223

Table 2
The variation of A_{pp}, B_{pp}, E_a, χ_o, C, θ, $\mu_{theo.}$ and $\mu_{cal.}$ for (Bi, Pb)-2223 and (Bi, Pb)-2212 phases versus Ru-content.

x	(Bi, Pb)-2223 phase							(Bi, Pb)-2212 phase						
	A_{pp} (G)	B_{pp} (G K^{-1})	E_a (eV)	χ_o (10^{-6}) emu/g	C (10^{-4}) emu K/g	θ (K)	μ_{theo} (μ_B)	$\mu_{cal.}$ (μ_B)	A_{pp} (G)	B_{pp} (G K^{-1})	E_a (eV)	χ_o (10^{-7}) emu/g	C (10^{-4}) emu K/g	θ (K)	$\mu_{theo.}$ (μ_B)	$\mu_{cal.}$ (μ_B)
0.0	274.51	0.0688	0.0161	2.43	3.81	−7.40	1.730	1.730	503.55	0.0617	0.0107	3.32	2.8	−7.96	1.730	1.723
0.025	268.91	0.0757	0.0169	2.23	4.49	−7.41	1.742	1.742	505.78	0.0595	0.0099	3.43	2.5	−7.94	1.748	1.747
0.05	265.11	0.0807	0.0176	2.11	5.03	−7.43	1.754	1.753	508.60	0.0525	0.0097	3.8	2.29	−7.92	1.766	1.765
0.075	279.41	0.0663	0.0150	1.52	2.79	−7.38	1.766	1.762	504.17	0.0497	0.0112	4.67	4.53	−7.99	1.784	1.783
0.15	–	–	–	–	–	–	–	–	503.89	0.0402	0.0116	8.08	5.61	−8.01	1.836	1.833
0.3	–	–	–	–	–	–	–	–	502.12	0.0380	0.0121	7.42	7.03	−8.04	1.935	1.934
0.4	–	–	–	–	–	–	–	–	500.02	0.0355	0.0126	7.52	8.86	−8.08	1.999	1.994

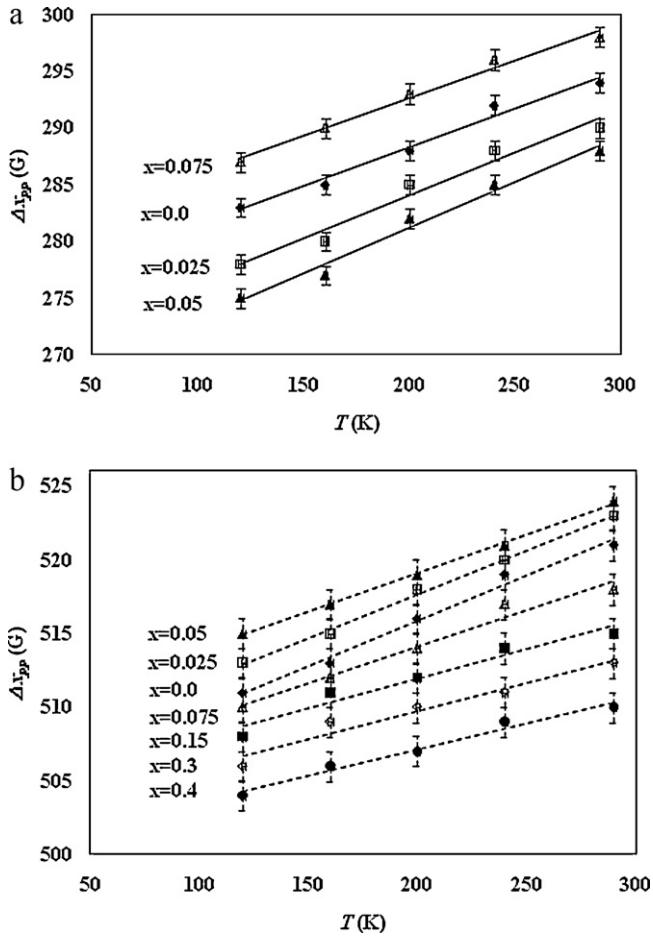

Fig. 7. The variation of Δx_{pp} with T for different Ru-content for (Bi, Pb)-2223 phase (a), and (Bi, Pb)-2212 phase (b).

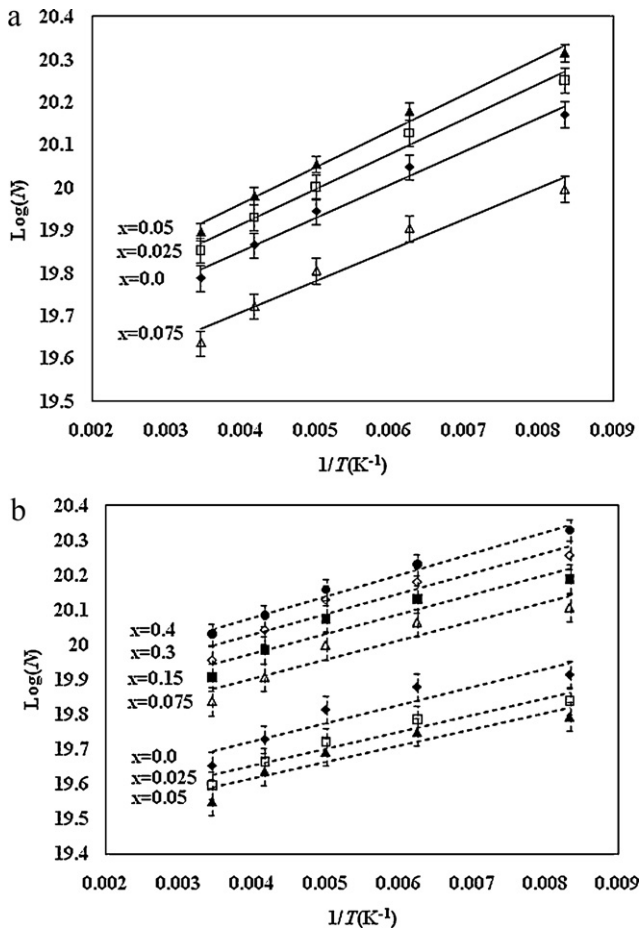

Fig. 8. The relation between log (N) and $1/T$ for different Ru-content for (Bi, Pb)-2223 phase (a), and (Bi, Pb)-2212 phase (b).

phase, could be attributed to the increase of the number of carriers in CuO_2-planes as Ru-content increased from 0.0 to 0.05 [16]. For (Bi, Pb)-2223 ($x = 0.075$) and (Bi, Pb)-2212 phases, the decrease in the value of B_{pp} is attributed to the partial substitution of Cu^{2+} ions by Ru^{4+} ions which increases the localization of charge carriers, and decreases the effective number of the carriers [31]. Moreover, this behavior is confirmed by the electrical resistivity data [16] which showed a semiconductor-like behavior as Ru-content increased. The semiconductor-like behavior was discussed according to Anderson impurity model [32]. This model shows that the electronic states near the Fermi surface are inerrant for a large overlap of the Cu (3d) and O (2p) wave-functions, but they become localized when this overlap was reduced.

A significant result has been observed when comparing the ratio between the area (A) under the EPR absorption curves of (Bi, Pb)-2223 and (Bi, Pb)-2212 phases with the volume fraction ratio of the same phases, which are nearly equal as shown in Table 1.

The number of spins N participating in the resonance for each phase can be calculated at different temperatures by comparing the area under the absorption curve with that of a standard one, using the following equation [26].

$$N = \frac{A_y(Scan_y)^2 G_{std}(B_m)_{std}(g_{std})^2[S(S+1)]_{std}(P_{std})^{0.5}}{A_{std}(Scan_{std})^2 G_y(B_m)_y(g_y)^2[S(S+1)]_y(P_y)^{0.5}} std \quad (7)$$

where $Scan$ is the magnetic field corresponding to unit length of the chart, G is the gain, B_m is the modulation field width, S is the spin of the system in its ground state and P is the power of the microwave.

The relation between logarithm N for (Bi, Pb)-2223 and (Bi, Pb)-2212 phases against the reciprocal of absolute temperature for different Ru-content is shown in Fig. 8(a) and (b), respectively. It is found that N increases as Ru-content increases from 0.0 to 0.05 and then it decreases at $x = 0.075$ for (Bi, Pb)-2223 phase. A reverse trend for the variation of N with Ru-content is observed for (Bi, Pb)-2212 phase. This behavior is consistent with that observed for XRD results, which showed a complete phase change from (Bi, Pb)-2223 phase to (Bi, Pb)-2212 phase at $x \geq 0.15$. It is also found that the number of spins decreases as the temperature increases for each phase at different Ru-content. A linear relation between log(N) and $1/T$ is found as expected from Boltzmann's law. The activation energy E_a values for each phase are calculated from the slope of lines, and listed in Table 2 versus Ru-content. The value of the activation energy of pure (Bi, Pb)-2223 phase is equal to that obtained for $Bi_{2-x}Pb_xSr_2Ca_2Cu_3O_{10+\delta}$ phase for $x = 0.3$ [33]. It is found for (Bi, Pb)-2223 phase that the value of E_a increases for small Ru-content until $x = 0.05$ and then it decreases at $x = 0.075$. This is attributed to the enhancement in its N values with increasing Ru-content until $x = 0.05$. While, the E_a value for (Bi, Pb)-2212 phase decreases as Ru-content increases until $x = 0.05$ and then it increases for $x \geq 0.075$. It is attributed to the decrement of the N values for (Bi, Pb)-2212 phase until $x = 0.05$, which then increase to be dominated for $x \geq 0.15$ [16]. Also, it can be due to the fluctuation of the valence state of Cu^{2+} ions as a result of the strong phase change from $n = 3$ phase to $n = 2$ phase.

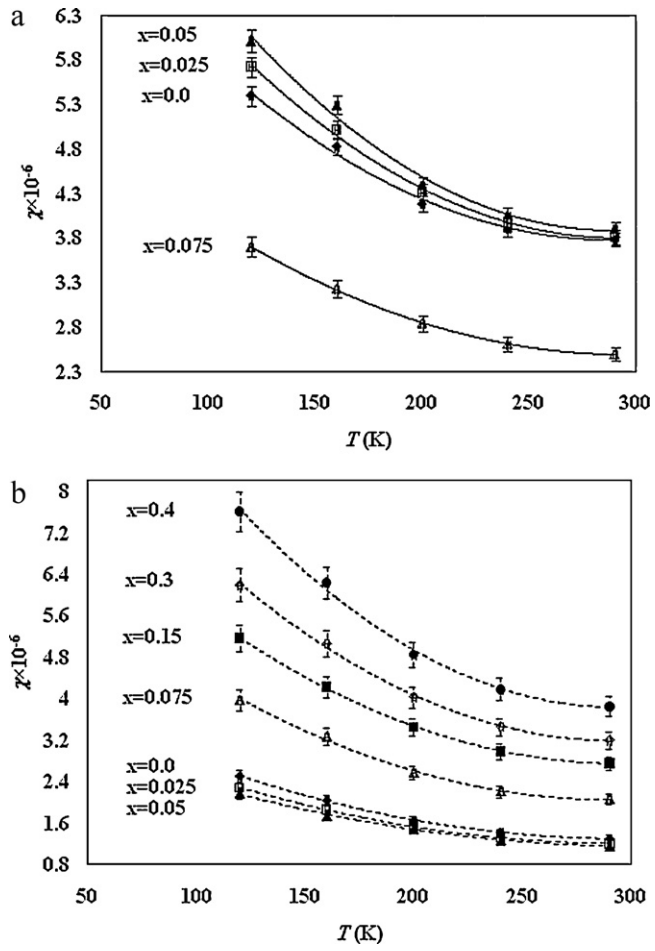

Fig. 9. The temperature dependence of the paramagnetic susceptibility for different Ru-content for (Bi, Pb)-2223 phase (a), and (Bi, Pb)-2212 phase (b).

The paramagnetic susceptibility χ is calculated for each phase at different temperatures using the following equation [34]:

$$\chi = \frac{Ng^2\beta^2 J(J+1)}{3k_B T} \tag{8}$$

where β is the Bohr magneton and J is total angular momentum. Fig. 9(a) and (b) shows the temperature dependence of the paramagnetic susceptibility at different Ru-content for (Bi, Pb)-2223 and (Bi, Pb)-2212 phases, respectively. The paramagnetic susceptibility is inversely proportional to the temperature and similar behavior of χ is observed for each phase with increasing Ru-content, where χ is directly proportional to N according to Eq. (8). The χ-T curves are well fitted according to Curie–Weiss law, using the following equation:

$$\chi = \chi_o + \frac{C}{T-\theta} \tag{9}$$

where χ_o is the temperature independent susceptibility, C is the Curie constant and θ is the Curie temperature. All the curves are well fitted to Eq. (9) in the temperature range from 120 to 290 K. The best fitting parameters for each phase are listed in Table 2. The listed values of C and θ for pure (Bi, Pb)-2223 and (Bi, Pb)-2212 phases are nearly equal to those reported for Bi-2223 and Bi-2212 phases, respectively [35]. Also, a similar behavior of C and θ as that for N and χ is observed for each phase with increasing Ru-content.

The calculated effective magnetic moment $\mu_{cal.}$ is obtained from the following equation:

$$C = \frac{N\mu_{cal.}^2}{3k_B} \tag{10}$$

The values of $\mu_{cal.}$ for each phase are listed in Table 2 versus different Ru-content. The theoretical magnetic moment, $\mu_{theo.}$, for each phase at different Ru-content can be calculated through the following expression [36]:

$$x\mu_{theo.}^2 = x_1\mu_{Cu^{2+}}^2 + x_2\mu_{Ru^{4+}}^2, \tag{11}$$

where x_1 and x_2 ($x_1 + x_2 = x$) are the equivalent molar concentration of Cu^{2+} and Ru^{4+} ions, respectively. The effective magnetic moment value of Cu^{2+} ions ($S = 1/2$) is 1.73 μ_B [37] and of Ru^{4+} ions ($S = 1$) is 2.83 μ_B [38]. The values of $\mu_{theo.}$, for each phase, are also listed in Table 2 versus Ru-content, which are comparable to the $\mu_{cal.}$ values. It is noticed that $\mu_{cal.}$, for each phase, increases as Ru-content increases. One can say that the partial replacement of Cu^{2+}ions by Ru^{4+} ions in CuO_2-planes yields an increase in the scattering of the induced magnetic moment of Cu atoms having Ru neighbor. The effective magnetic moment for (Bi, Pb)-2223 phase substituted by Fe [39] is higher than that substituted by Ru, at the same content $x = 0.05$. This means that Fe-substitutions are more effective than Ru-substitutions to increase the scattering of that induced magnetic moment of Cu atoms. This is because the effective magnetic moment of Fe^{5+} ions (5.9 μ_B) is higher than that of Ru^{4+} ions (2.83 μ_B).

4. Conclusions

The EPR spectra of Cu^{2+} ions in $Bi_{1.8}Pb_{0.4}Sr_2Ca_{2.1}Cu_{3-x}Ru_xO_{10+\delta}$ ($0.0 \le x \le 0.4$) were measured from room temperature down to 120 K. The EPR spectra, for $0.0 \le x \le 0.075$, showed two lines, indicating the formation of both (Bi, Pb)-2223 and (Bi, Pb)-2212 phases. Only one line, corresponding to (Bi, Pb)-2212 phase, appeared for $x \ge 0.15$. This could be attributed to the phase change from (Bi, Pb)-2223 phase to (Bi, Pb)-2212 phase which was confirmed by our previous work through XRD and electrical resistivity measurements. The g-values for both phases showed a slight decrement as the temperature decreased from room temperature to 120 K. A correlation between the fitting parameters, determined from the temperature dependence of the peak-to-peak line width, and both of the volume fraction of the two phases and the carriers density, determined from the XRD and the electrical resistivity, was observed. For (Bi, Pb)-2223 phase, both number of spins N and activation energy E_a increased as x increased from 0.0 to 0.05 followed by a decrease in their values with further increase in x. A reverse trend for the variation of both N and E_a with x was found for (Bi, Pb)-2212 phase. The effective magnetic moment increased as x increased for both phases, indicating that the partial replacement of Cu^{2+} ions by Ru^{4+} ions caused an increase in the scattering of the induced magnetic moment of Cu atoms having Ru neighbor.

References

[1] M. Cyrot, D. Pavuna, Introduction to Superconductivity and High-T_c Materials, World Scientific, Singapore, 1995, p. 249.
[2] G. Blatter, M.V. Feigelman, V.B. Ceshkenbein, A.I. Larkin, V.M. Vinokur, Rev. Mod. Phys. 6 (1994) 1125.
[3] F. Marti, G. Grasso, J.-C. Grivel, R. Flükiger, Supercond. Sci. Technol. 11 (1998) 485.
[4] K. Watanabe, M. Kojima, Supercond. Sci. Technol. 11 (1998) 392.
[5] V. Garnier, I. Monot-Laffez, G. Desgardin, Physica C 349 (2001) 103.
[6] A.L. Crossley, Y.H. Li, A.D. Caplin, J.L.M. Drisoll, Physica C 314 (1999) 12.
[7] H. Maeda, Y. Tanaka, M. Fukutomi, T. Asano, Jpn. J. Appl. Phys. 27 (1988) L209.
[8] Y.T. Huang, D.S. Shy, L.J. Chen, Physica C 294 (1998) 140.
[9] C.Y. Shieh, Y. Huang, M.K. Wu, C.Y. Huang, Physica C 185–189 (1991) 513.
[10] S.A. Halim, S.A. Khawaldeh, H. Azhan, S.B. Mohamed, K. Khalid, J. Suradi, J. Mater. Sci. 35 (2000) 3043.

[11] A. Tampieri, G. Celotti, S. Lesca, G. Bezzi, T.M.G. La Torretta, G. Magnani, J. Eur. Ceram. Soc. 20 (2000) 119.
[12] C.N.R. Rao, L. Ganapathi, R. Vijayaraghavan, G.R. Rao, K. Murthy, R.A. Mohan Ram, Physica C 156 (1988) 827.
[13] P. Kameli, H. Salamati, I. Abdolhosseini, J. Alloys Compd. 458 (2008) 61.
[14] C. Terzioglu, M. Yilmazlar, O. Ozturk, E. Yanmaz, Physica C 423 (2005) 119.
[15] S.E. Mousavi Ghahfarokhi, M. Zargar Shoushtari, Physica B 405 (2010) 4643.
[16] A.I. Abou-Aly, R. Awad, S.A. Mahmoud, M.M.E. Barakat, J. Supercond. Nov. Magn. 23 (2010) 1575.
[17] C. Terzioglu, J. Alloys Compd. 509 (2011) 87.
[18] H. Abbasi, J. Taghipour, H. Sedghi, J. Alloys Compd. 494 (2010) 305.
[19] D. Shaltiel, H.-A. Krug von Nidda, B.Ya. Shapiro, B. Bogoslavsky, B. Rosenstein, I. Shapiro, T. Tamegai, Physica C 470 (2010) 1937.
[20] V.A. Ivanshin, I.N. Kurkin, E.V. Pomjakushina, Phys. Solid State 51 (2009) 322.
[21] S.-Y. Wu, G.-D. Lu, H.-M. Zhang, Z.-H. Zhang, Physica C 466 (2007) 163.
[22] L. Bejjit, M. Haddad, Physica C 371 (2002) 339.
[23] X.-G. Li, X. Sun, W. Wu, Q. Chen, L. Shi, Y. Zhang, Y. Kotaka, K. Kishio, Physica C 279 (1997) 241.
[24] F.J. Owens, Z. Iqbal, A.A. Zakhidov, I.I. Khairullin, Physica C 174 (1991) 309.
[25] I. Felner, U. Asaf, Y. Levi, O. Millo, Phys. Rev. B 55 (1997) 3374.
[26] J.A. Weil, J.R. Bolton, Electron Paramagnetic Resonance-Elementary Theory and Practical Applications, Second ed., John Wiley & Sons, Inc., Hoboken, New Jersey, 2007.
[27] M.C.M. O' Brien, Proc. R. Soc. Lond. 281 (1964) 323.
[28] M.J. Riley, M.A. Hitchman, D. Reinen, Chem. Phys. 102 (1986) 11.
[29] S.E. Barnes, Adv. Phys. 30 (1981) 801.
[30] H. Shimizu, K. Fujiwara, K. Hatada, Physica C 282–287 (1997) 1349.
[31] A.I. Abou-Aly, N.H. Mohammed, R. Awad, I.H. Ibrahim, Supercond. Sci. Technol. 13 (2000) 1107.
[32] H. Eskes, G.A. Sawatzky, Phys. Rev. Lett. 61 (1988) 1415.
[33] A. Sedky, A.M. Ahmed, Chin. J. Phys. 41 (2003) 511.
[34] N.W. Aschcroft, N.D. Mermin, Solid State Physics, Harcourt College Publishers, 2001.
[35] T. Ishida, K. Kanoda, T. Takahashi, K. Koga, Physica C 178 (1991) 231.
[36] S. Simon, R. Pop, V. Simon, M. Coldea, J. Non-Cryst. Solids 331 (2003) 1.
[37] Y. Ono, K.-i. Satoh, T. Nozaki, T. Kajitani, Jpn. J. Appl. Phys. 46 (2007) 1071.
[38] A. Butera, M. Vásquez Mansilla, A. Fainstein, G.V.M. Williams, Physica B 320 (2002) 316.
[39] A.V. Pop, Gh. Ilonca, D. Ciurchea, M. Ye, I.I. Geru, V.G. Kantser, V. Pop, M. Todica, R. Deltour, J. Alloys Compd. 241 (1996) 116.